Robotic Manipulators Performing Smart Sanding Operation: A Vibration Approach

Joshua Nguyen[1], Manuel Bailey[1], Ignacio Carlucho[1] and Corina Barbalata[1]

***Abstract*— This paper presents the design of a novel expert system for robotic manipulators performing sanding tasks on work surfaces. The expert system adjusts the velocity of the robotic manipulator based on the estimated surface quality. These estimations are obtained by a real-time analysis of the raw force data provided by a force-torque sensor at the end-effector level. The expert system consists of two governing control laws that act in parallel, a variable velocity generation law and a pose regulation-based law. The variable velocity law regulates the velocity of the manipulator along a set path, in the tangent direction, based on an analysis of the frequency and amplitude of the force signal generated during the sanding process. The pose regulation-based law drives the manipulator in the bi-normal and rotational direction, ensuring the manipulators remain on the sanding path with the desired orientation. The proposed strategy is experimentally evaluated using the UR5e collaborative robotic manipulator sanding wood and metal panels. The obtained results show that such an approach is beneficial to ensure accurate contact between the sanding tool and the working environment, robust path tracking, and smart sanding.**

I. Introduction

Finishing operations, such as trimming, surface treatment, grinding, sanding, and painting, are necessary to ensure components possess required geometrical tolerances and properties [1]. Sanding and polishing represent two of the most common finishing processes, both of which are processes that remove small amounts of material on a components surface [2]. As presented in [3] the sanding process is common in furniture manufacturing, where it is used to remove residuals caused by wood processing to ensure homogeneously smooth parts. These operations can be costly and time-consuming [4]. Furthermore, for human operators, those tasks are tedious, leading to physical discomfort and repetitive strain injuries, risks that could be mitigated by an automated solution [5]. Robotic systems represent a solution that both decrease cost and improve the sanding process. The state-of-the-art in robotic sanding technology has followed two avenues: 1) autonomous sanding where the path and the velocity along the path are predefined or 2) teleoperated robotic sanding that leverages the knowledge of a human operator to monitor and intervene in the process described in the previous point and remove individual flaws [6]. Nevertheless, these approaches have limited applicability for wide deployment as they rely on human-expertise and do not account for part variability. To enable fully autonomous robotic systems to be deployed in sanding operations, the following barriers have to be addressed: 1) the motions for sanding cannot be planned prior to the sanding process, as residual stresses during manufacturing may cause dimensional variations in the final parts geometry by up to several centimeters [7]; 2) both the nature and duration of the tasks to be performed vary from one part to another because of the aforementioned variability that occurs during manufacturing; and 3) task completion is based on a human operator's judgement and previous experience, which is difficult to automate.

Fig. 1: UR5e collaborative manipulator with specialized sanding tool as its end-effector.

In order to address these barriers, in this work we design a smart framework for achieving variable velocity motion of the robotic manipulator based on surface quality. The main contributions of this framework are: 1) establishing a correlation between vibration information and surface quality using only a force/torque sensor and 2) the design of an expert system that results in variable velocity motion profiles while regulating the contact force with the environment. The proposed architecture will enable robotic manipulators with specialized sanding tools (Figure 1) to achieve high-quality sanding without human-input, using information only from the sensors integrated in the robotic manipulator.

The reminder of this paper is structured as follows. Background information on sanding and control systems used in sanding applications are presented in Section II. The proposed strategy is presented in detail in Section III. The results of the proposed strategy are shown in Section IV and

[1]Joshua Nguyen, Manuel Bailey, Ignacio Carlucho, and Corina Barbalata are with the Department of Mechanical & Industrial Engineering, Louisiana State University, Baton Rouge, LA 70803, USA jngu114@lsu.edu; mbail37@lsu.edu; icarlucho@lsu.edu; cbarbalata@lsu.edu

are followed by the conclusions in Section V.

II. Related Work

One of the core aspects that allows for the autonomy of a smart robot is its control system [8]. The general rule in sanding tasks is that passive force control cannot achieve high enough precision for these processes to be applicable [1]. The Preston equation [9] shows that the contact pressure and the rotary speed of the cutting tool is related to the material removal rate of a work piece [10], [11]. Combining this with the Hertz contact theory [12] which relates contact forces, material properties, and geometries of contacting bodies to contact pressure, it shows that force regulation directly affects the material removal rate. The authors of [13] state that high quality sanding is achieved by pressure regulation, which can be achieved by force regulation. To reach high-precision force regulation, a feedback control system is needed, and the most common and accurate method to control the tool is done via active force control. Typically, in sanding application, the rotary speed of the tool is set constant and thus the material removal rate becomes dependent on the force the tool applies normal to a work piece [10]. Initial studies in deploying collaborative robotic manipulators in finishing operations are presented in [14]. The goal of these works is to investigate both open-loop and closed-loop force control structures and their impact on the quality of finish. It was concluded that accurate force regulation improves the quality of the sanding, but an increase in the contact force does not ensure a better finish. A sliding mode controller is implemented in [15] and used for the force regulation in a hybrid force-motion controller, while for position control, a state-of-the-art continuous tracking controller is used. The advantages of this method are its robustness and its low-computational cost. In [1] fuzzy logic is incorporated into the force portion of a hybrid force-motion controller. Depending on the force error, the fuzzy logic adjusts the Proportional-Integral-Derivative (PID) controller gains in the force regulator to adapt the behavior of the polishing tool onto the environment. The authors in [16] use motor encoders and joint-torque sensors to estimate the normal force applied to the work surface and build a hybrid force-motion controller using that estimation. This is shown to be a useful alternative to the typical force-torque sensor attached to the end-effector. Furthermore, the paper also implements a vibration filter during data processing to better improve force estimation. In [17] and [18] an acoustic emission sensor is used to estimate the surface roughness, tool wear, and to adjust the polishing force and tool speed accordingly.

In [19] it has been shown that there is a relationship between the vibrations sensed and the roughness of a surface for a polishing/sanding task. The authors investigate the force signals created during the task. The paper concluded that the force signals became more variant as the surface became smoother. Knowing this, the force signal characteristic was able to give indication onto the state of the surface under the tool in real time. In [20] it is concluded that the shear forces/stresses play no significant part in polishing/sanding applications and [21] states that the normal force and feed rate need to be considered for good results. Another common limitation in current automated polishing and sanding is the lack of adaptability and flexibility. Many robotic polishing/sanding systems rely on CNC machines that are either costly or specialized for only small items [22]. In [23] a deformation-based trajectory optimization strategy is proposed for the motion of an industrial arm, considering the velocity constraints to improve the quality of the finishing operation. The velocity constraints are determined based on the deformation analysis. A constant velocity approach is presented in [6] where the authors propose a human-machine framework for sanding of complex surfaces. The robot is driven by a programming-by-demonstration strategy where experienced human workers manually show the robot how to perform sanding.

The most significant disadvantages of the methods shown above are the lack of real-time surface estimation of the surface roughness, the use of constant sanding velocity profiles, and the need of human operators in assessing the quality of the sanding. All of these restrict the advancements in achieving highly autonomous sanding using robotic systems. To address these limitations, we propose a framework that facilitates smart sanding with robotic systems by: 1) characterizing the correlation between vibration and surface roughness using only a force-torque sensor and 2) designing an expert system using vibration-based control laws for generating variable velocity profiles for the manipulator, ensuring contact force regulation.

III. Methodology

A. Vibration estimation and roughness correlation

To establish a correlation between vibrations and surface roughness using only a force/torque sensor attached to the end-effector of the manipulator, an analysis of the force signal is presented in the following paragraphs.

Force measurements taken at the end-effector, with an integrated force-torque sensor, during the sanding process are inherently noisy due to the vibrations caused by the sander's motor and the rough surface that is being sanded [24]. Because of this, it is recommended to look at the force signal in the frequency domain. This is done by transforming the force signal using the Fast-Fourier Transform (FFT) [25]. An example of the FFT graph produced during sanding can be seen in Figure 2. The force-torque sensor samples at a rate of 500 Hz, at each time step we utilized a window of one second of previous data to calculate the FFT. It can be seen that when the sander is turned on, regardless if the tool is in the air or in contact with the environment, vibrations are present. The frequency of these vibrations depend on both the tool and the working surface if the tool is in contact with the surface. As the sander makes contact with the surface, the surface dampens the vibration frequency while increasing the magnitude of the vibration. As the surface gets smoother, the dampening effect increases and the amplitude begins to diminish. This behavior has been

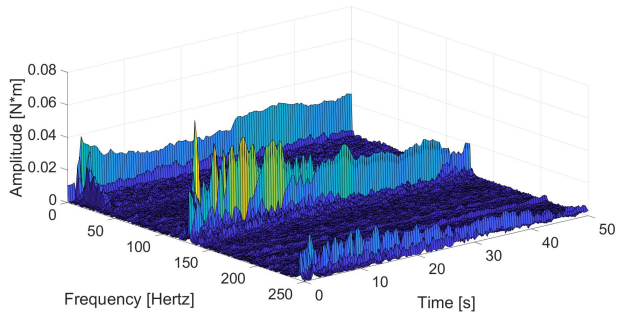

Fig. 2: Fast-Fourier Transform (FFT) of the measured normal torque when the sanding tool is on.

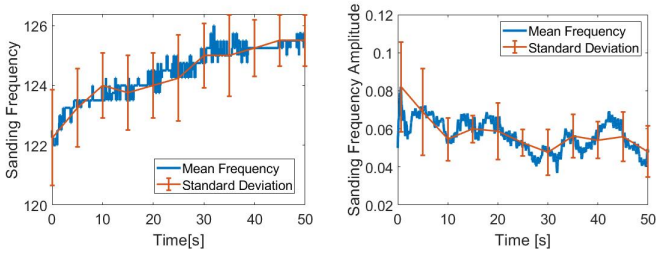

(a) (b)

Fig. 3: FFT components analysis: average and standard deviation for (a) sanding frequency vs. time and (b) amplitude of frequency vs time.

observed across several experiments, where the robotic arm was commanded to sand a singular area while maintaining a normal force of 15N for 50 seconds. The average value and standard deviation of the sanding frequency and its amplitude have been computed across all these experiments. As seen in Figure 3, this analysis validates the assumption that sanding frequency increases over time and the amplitude decreases over time, indicating a less rough surface. Furthermore, similar behaviour has been shown in [19] where a relationship between surface roughness of an alloy steel and force data coming from gauge sensor was found. The study shows that the frequency analysis of the force data could be potentially used to estimate the surface roughness, however, the study does not utilize this information for online estimation of the roughness. It is this relationship that allows for an online surface estimation and what is used to establish governing control laws for the proposed expert system.

B. Expert system design

a) Coordinate frame definition: The proposed expert system is designed based on the local coordinate system of the working surface. In this paragraph we describe this coordinate system, known as the *n-t* coordinate system or the path coordinate system, and its usage for the design of the proposed architecture. When the tool of the manipulator moves along a path (curved or straight), it can be convenient to describe its motion using the normal, tangential and bi-normal coordinate system, also known as *n-t* coordinate system, and not the classical Cartesian coordinate system. We define a path coordinate system where the tangent unit vector, t, maintains a direction along the path on the surface while the normal unit vector, n, is aligned with the normal of the surface at the current location of the tool. The bi-normal unit vector, b, is determined by the right-hand rule such that $b = t \times n$. Figure 4 shows the path coordinate system in the set-up of sanding tasks for flat surfaces. It has to be noted that the manipulator used in this research only accepts commands in its base coordinate frame. To accommodate this, the velocity signal that is developed in the path coordinate frame is transformed into the base coordinate Cartesian frame, leading to the commanded end-effector's linear and angular velocities given by $v_c = [v_x,\ v_y,\ v_z,\ v_\psi,\ v_\theta,\ v_\theta]^T$. The transformation between the *n-t* coordinate system and the Cartesian coordinate system is given by $[v_x,\ v_y,\ v_z,\ v_\psi,\ v_\theta,\ v_\theta]^T = R(\cdot) \cdot [v_t,\ v_n,\ v_b,\ v_\alpha,\ v_\beta,\ v_\gamma]^T$, where $R(\cdot)$ is the rotation matrix between the $n-t$ coordinate frame and the Cartesian frame. v_n is the velocity in the normal direction, set to a constant value and v_t, v_b, v_α, v_β, v_γ are the outputs of the expert system presented in the following paragraphs.

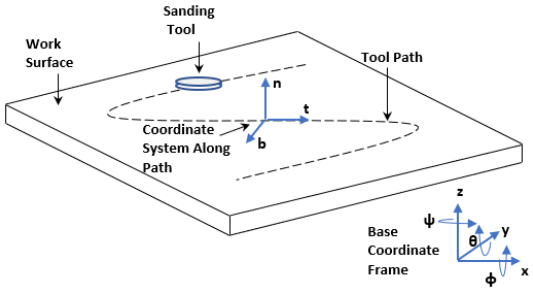

Fig. 4: Motion of the sanding tool on the work surface, describing the coordinate systems used.

b) Governing control laws: The proposed expert system architecture, seen in Figure 5 drives the velocity profile in the *n-t* coordinate system. The system has two governing control laws: 1) a pose-driven control law and 2) a vibration-driven control law. The pose-driven control law commands the end-effector in the ϕ-, θ-, ψ- axes and in the bi-normal axis. While the vibration-driven law does it in the tangential axes. This structure ensures that the sanding tool is not deviating from the desired path and at the same time effectively sands the rough areas. This is done by controlling the velocity based on the measured vibration estimation, ensuring that a single pass over an area is sufficient to achieve smooth surfaces. The individual components of the system are presented in the following paragraphs.

Vibration-driven control law: The proposed vibration-driven control law is responsible for the definition of the tool's velocity in the tangential direction to the work piece along a given path. Based on the vibration-roughness correlation presented in Section III-A, the proposed vibration-driven control law output is inversely proportional to the amplitude and frequency information. Specifically, as the surface becomes smoother the velocity of the end-effector should increase, as the robot should spend less time sanding those areas. The formulation of the vibration-control law is

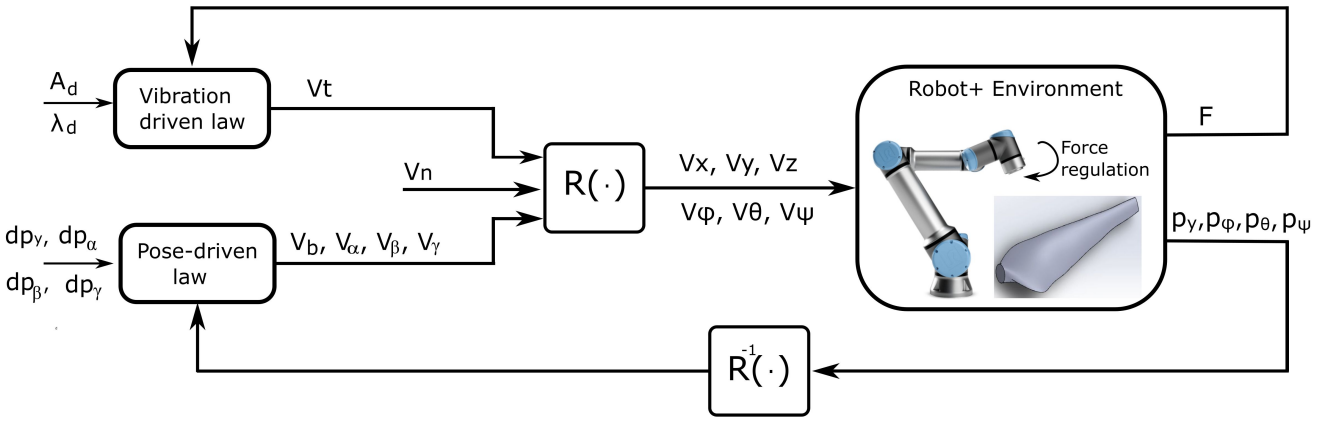

Fig. 5: The proposed expert system: the vibration-driven control law acts in the tangent axes based on the FFT information, the pose-driven control law acts in the ϕ-, θ-, ψ- axes and in bi-normal axis, The rotation matrix transforms the *n-t* coordinate frame to the base Cartesian coordinate frame and an internal force regulator is used in the UR5e robot.

given by:

$$\begin{aligned} v_t &= \frac{1}{u_\lambda + u_A} \\ u_\lambda &= K_\lambda \cdot e_\lambda, \quad u_A = K_A \cdot e_A \\ e_\lambda &= \lambda_m - \lambda_d, \quad e_A = A_d - A_m \end{aligned} \tag{1}$$

where λ_d is the the free spin sanding frequency that is dependent on the sanding tool used, and λ_m is the measured sanding frequency taken from the FFT. The measured sanding frequency is taken to be the frequency with the highest amplitude within a predefined range. The frequency range is determined empirically based on the properties of the work surface, sanding tool, and sand paper grit size. A_d is the free spin amplitude of the sanding frequency that is dependent on the tool used. A_m is the measured amplitude of the sanding frequency determined above. e_λ represents the error in frequency domain and e_A is the error in amplitude, K_A is the normalization factor for the amplitude component of the controller and K_λ is the normalization factor for the frequency component. v_t is the commanded velocity in the tangent-axis and is set such that if there is a large error in lambda (e_λ), or the amplitude (e_A), the velocity v_t will be low. A large e_λ or e_A indicates a rough surface, meaning more sanding is required.

The magnitude of the frequency dampening effect and the amplitude increase depend on the sanding parameters used for sanding. The proposed vibration-based control law uses a combination of the measurement of both the dampening effect and amplitude increase and is shown in Equation (1). By combining the information provided by both parameters we ensure meaningful information is received by the expert system, achieving a reliable sanding behaviour. As presented in [19] this can happen for several materials including alloy steel. The control signals u_λ and u_A, are added together to limit the effects in case one of the control signals is near zero, which would cause issues since the vibration-based component control law is inversely proportional to the amplitude and frequency information.

Pose-based control law: The pose-based controller is responsible for determining the angular velocity of the end-effector and the bi-normal velocity with respect to the path. This component ensures that the sanding tool does not deviate from the predefined path and orientation by rapidly driving the manipulator back if it senses a difference between its position and the path. The pose based-formulation uses two parallel rules, one for angular velocity computation and another for the bi-normal velocity formulation. The angular velocity component is a Proportional-Derivative (PD) controller described by:

$$e_p = d_p - p, \quad v_p = K_{p,p} \cdot e_p + K_{d,p} \cdot \dot{e}_p \tag{2}$$

where $p = [\ p_\alpha,\ p_\beta,\ p_\gamma]^T$ is the end-effector orientation in normal, bi-normal and tangential directions; $d_p = [\ d_{p_\alpha},\ d_{p_\beta},\ d_{p_\gamma}]^T$ is the desired orientation of the end-effector in the normal, bi-normal, and tangential directions. $K_{p,p}$ and $K_{d,p}$ are 3×3 diagonal matrices representing the gains of the controller. The output of the controller is the commanded velocity $v_p = [\ v_\alpha,\ v_\beta,\ v_\gamma]$ consisting of the angular velocities. This control structure was chosen to ensure a smooth motion of the end-effector avoiding any overshoot and robust transient response.

The bi-normal velocity component is designed for maintaining the tools position along the path, using the position error in the bi-normal direction. The controller architecture takes the form of:

$$\begin{aligned} e_b &= d_b - b \\ v_b &= K_{p,b} \cdot e_b + K_{i,b} \int e_b dt + K_{d,b} \cdot \dot{e}_b \end{aligned} \tag{3}$$

where v_b is the velocity in the bi-normal direction, $K_{p,b}$, $K_{i,b}$, and $K_{d,b}$ are the gains of the controller, and e_b is the error in position in the bi-normal direction, defined by the desired position in the bi-normal direction d_b and the current

	Wood						Steel		Aluminum			
Experiment #	1	2	3	4	5	6	7	8	9	10	11	12
Before	15.16	18.71	14.16	16.56	17	16	554	320.3	1.011	0.7415	3.348	1.445
Proposed	12	8.8	8.31	9.17	7.71	11.52	176.8	204	0.5596	0.6066	1.004	0.8086
Constant	13.13	9.46	8.76	14.53	11.49	13.59	187.86	199.87	0.7631	0.6517	1.178	0.9381
Performance Diff.	16.91	105.11	64.98	22.13	71.4	20.92014	207.1	59.03	44.29	14.80	216.13	62.68
Mean Perform. Diff	13.61%						0.35%		10.09%			

TABLE I: Roughness measurements for wood, steel and aluminium samples: before sanding, after sanding using the proposed variable velocity approach, and using a constant velocity as presented in [6].

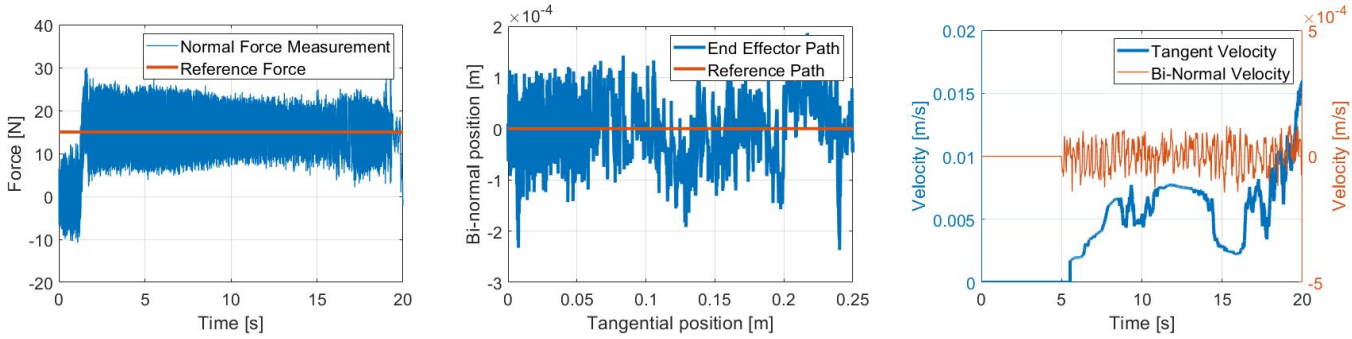

(a) (b) (c)

Fig. 6: The end-effector behaviour using the proposed expert system: (a) contact force measured during sanding, (b) the end-effector position in the bi-normal and tangential coordinate system, (c) the velocity of the manipulator in the tangent and bi-normal direction

position b. For this application we consider that the desired position in the bi-normal direction is zero as we do not wish for the tool to stray off of the planned path.

C. Force regulation

The force regulator is responsible for maintaining the desired force in the normal direction during sanding. With the use of the UR5e for testing, the UR5e implements its own force control algorithm and is used in tandem with the governing control laws. The UR5e's force regulator accepts a user input of the desired force and the direction on which this force has to be applied.

IV. Results

For experimentation setup, a UR5e robot from Universal Robotics was used. A Makita XOB01T orbital sander was attached to the UR5e's force-torque sensor located at the end-effector using a custom made 3D printed bracket. The force-torque sensor allows for the force measurement in the three spatial direction and torque measurement in the three rotational directions. The orbital sander speed was set to 9,500 orbits per minute for each test. The sanding speed is fixed by the manufacturer and cannot be adaptively controlled. A 127 mm diameter 80 grit sand paper pad was attached to bottom of the sander and blocks of wood and metal were used as the sanding surface, as seen in Figure 7. The surfaces vary in size with a minimum width and length of 140 mm and 480 mm respectively. The proposed expert system was implemented and data was recorded using the UR5e's Real Time Data Exchange network protocol with the use of an externally connected Microsoft Surface laptop using Python. The Numpy library was used for the analysis of the force signal using FFT [26].

During the experimental testing, the manipulator was tasked with applying and maintaining a 15 N reference force, and moved along the block of wood/metal (Figure 7) while the orbital sander was operational. The path of the sander was a straightforward path of $25cm$. The proposed architecture was compared to the baseline approach in sanding, such as the one presented in [6], where the manipulator moves at a constant velocity along the work surface. For consistency, each experiment ran both approaches on the same block of wood/metal but at different locations. The proposed strategy was ran first for each of the n experiments. We then calculated the mean tangential speed for that particular experiment ($\overline{v}_t^n$). This value was then used as the requested velocity for the constant velocity tests for the corresponding n experiment. A Micro Photonics Nanovea optical profilometer was used to measure the roughness of wood/metal before and after sanding for each controller.

A. Experimental Results

This section presents the results obtained when the proposed approach has been tested in the environment described in the previous paragraph. Table I shows the results of the experiments performed on wood and metal blocks. The first six experiments were performed on wood, and the last two were performed on metal. The mean roughness measurements were obtained with the optical profilometer described previously. The table shows the average of three random measurements taken by the profilometer on the work surface. The optical profilometer scans a 2mm x 2mm area and measures the distance between the scanned area and a light source. This provides an elevation map of the scanned areas, from which, the surface roughness can be calculated.

The surface roughness of the area is calculated using:

$$S_a = \frac{1}{A} \int^{A} \mid z \mid dA \tag{4}$$

where A is the area of the measured surface and z is the difference in height from the average height of the measured surface. The performance difference metric was calculated by taking the difference between the after roughness of the proposed approach and the constant velocity approach and dividing by the original roughness. The metric directly compares how well the proposed controller is able to decrease surface roughness with the constant velocity controller.

From Table I it can be seen that the proposed approach was successfully able to decrease the surface roughness of the environment. Furthermore, the mean surface roughness after sanding shows that the expert system performs better than a constant velocity approach. In experiment 8 the proposed approach was slightly worse compared to the baseline strategy. This may be caused by the natural irregularities found in metal and particularly in this singular specimen.

Figure 6a shows the overall behavior of the end-effector tool when the proposed approach is used to sand the environment. It can be seen that the end-effector is maintaining a constant force, it is doing a single pass over the area to be sanded but at a variable velocity. Specifically, Figure 6a shows that the desired force (15 N) in the normal axis is achieved and maintained throughout the entire sanding process. The beginning of the graph presents force oscillations around 0 N, showing that the manipulator had yet to make contact with the surface. These oscillations are mainly due to the vibrations of the sander. After 2 seconds, the graph shows the sander achieves contact with the surface. This force is maintain for the duration of the experiment. Figure 6b shows the recorded motion versus reference path for the end-effector, displayed in the tangential - bi-normal axes. The proposed approach ensures the position along the path is maintain, the error in the path being negligible to the degree of 10^{-4} meters. Figure 6c shows the tangential and bi-normal velocity of the manipulator over time. The velocities are set to 0 m/s until the UR5e's force-torque sensor measures a 15 N contact force. This graph shows how the robotic arm velocity needs to be adjusted when the system detects a rougher surface. At the 14 second mark in this graph, the system detects that it is in contact with a rough surface and decreases the tangential velocity to maintain its location. Once the controller senses that the surface is smooth, it then increases its tangential velocity to the end of the path. The velocity in the bi-normal direction is small in comparison to the tangential velocity due to the lack of a deviation in the bi-normal position.

The proposed approach's main advantages is that it is able to sand a given surface intelligently and improve surface finish performance when compared to a constant speed approach. The force measurements and tangential velocity may also indicate the conditions of the surface without the need of a profilometer, and simply relying on a force/torque sensor placed at the end-effector of the robotic arm. Furthermore, the simplicity of the system allows for real-time implementation. The main limitation of this approach is that prior information about the vibration characteristics are needed for every specific material, which may not be readily available. Another limitation is that the proposed approach requires more time to complete the sanding operation. Nevertheless, in industrial settings, human operators require to have multiple passes over the same area to obtain high quality sanding.

Fig. 7: Wood and metal sample blocks used for testing.

V. Conclusion

This paper presents a smart system for autonomous sanding operations with robotic manipulators. The proposed strategy is based on the correlation found between vibrations and surface roughness. An analysis using the FFT of the forces measured with a force/torque sensor is performed, showing the correlation between the sanding frequency and the amplitude of the frequency with the surface roughness. Additionally, an expert system consisting of a vibration-driven and a pose-driven control law is presented. The system leverages the surface roughness estimation performed with the FFT to adjusts the velocity of the end-effector based on the roughness of the area to be sanded. This formulation allows for an adaptive velocity, which ensures reliable sanding with one single pass of the end-effector.

The results show that the proposed strategy is able to ensure an adequate sanding of different flat surface materials. Furthermore, a comparison with a constant speed controller shows that our proposed control strategy is able to obtain a smoother surface. Future work will investigate the possibility of extending the controller to surfaces of different shapes. Additionally, a smart motion planning algorithm will be integrated with the controller to improve the sanding trajectory.

Acknowledgements

This work has been funded by the National Science Foundation Award Number 2024795, "NRI: FND: Collaborative Mobile Manufacturing in Uncertain Scenarios".

REFERENCES

[1] Zhang, H., Li, L., Zhao, J., Zhao, J., Liu, S., and Wu, J., 2020. "Design and implementation of hybrid force/position control for robot automation grinding aviation blade based on fuzzy pid". *The International Journal of Advanced Manufacturing Technology,* ***107***(3), pp. 1741–1754.

[2] Luo, B., Li, L., Liu, H., Xu, M., and Xing, F., 2014. "Analysis of sanding parameters, sanding force, normal force, power consumption, and surface roughness in sanding wood-based panels". *BioResources,* ***9***(4), pp. 7494–7503.

[3] Leite, S. S., Jesus, G. M. K., de Sampaio Alves, M. C., de Domenico Valarelli, I., Moizes, F. A., and Salvadeo, V. M., 2019. "Experimental investigation of parameters impacting the roughness of pinus elliottii wood". *BioResources,* ***14***(1), pp. 2051–2061.

[4] Giublin, B., Vieira, J. A., Vieira, T. G., Trabasso, L. G., and Martins, C. A., 2014. "Experimental analysis of the automated process of sanding aircraft surfaces". *The Aeronautical Journal (1968),* ***118***(1199), p. 53–64.

[5] Mohsin, I., He, K., Li, Z., and Du, R., 2019. "Path planning under force control in robotic polishing of the complex curved surfaces". *Applied Sciences,* ***9***(24), p. 5489.

[6] Maric, B., Mutka, A., and Orsag, M., 2020. "Collaborative human-robot framework for delicate sanding of complex shape surfaces". *IEEE Robotics and Automation Letters,* ***5***(2), pp. 2848–2855.

[7] Trudeau, P., Demaria, C., Palardy, G., Salek, H., Jette, M.-A., and Hubert, P., 2013. "Process induced deformation of aircraft structural components". In 19th International Conference on Composite Materials.

[8] Hernández, B., and Giraldo, E., 2018. "A review of path planning and control for autonomous robots". In 2018 IEEE 2nd Colombian Conference on Robotics and Automation (CCRA), IEEE, pp. 1–6.

[9] Preston, F., 1927. "The theory and design of plate glass polishing machines". *Journal of Glass Technology,* ***11***(44), pp. 214–256.

[10] Tian, F., Li, Z., Lv, C., and Liu, G., 2016. "Polishing pressure investigations of robot automatic polishing on curved surfaces". *The International Journal of Advanced Manufacturing Technology,* ***87***(1), pp. 639–646.

[11] Wang, Q.-H., Liang, Y.-J., Xu, C.-Y., Li, J.-R., and Zhou, X.-F., 2019. "Generation of material removal map for freeform surface polishing with tilted polishing disk". *The International Journal of Advanced Manufacturing Technology,* ***102***(9), pp. 4213–4226.

[12] Zhang, L., Tam, H., Yuan, C., Chen, Y., and Zhou, Z., 2002. "An investigation of material removal in polishing with fixed abrasives". *Proceedings of the Institution of Mechanical Engineers, Part B: Journal of Engineering Manufacture,* ***216***(1), pp. 103–112.

[13] Huissoon, J., Ismail, F., Jafari, A., and Bedi, S., 2002. "Automated polishing of die steel surfaces". *The international journal of advanced manufacturing technology,* ***19***(4), pp. 285–290.

[14] Ubeda, R. P., Gutiérrez Rubert, S. C., Stanisic, R. Z., and Perles Ivars, Á., 2021. "Behavioural study of the force control loop used in a collaborative robot for sanding materials". *Materials,* ***14***(1), p. 67.

[15] Solanes, J. E., Gracia, L., Muñoz-Benavent, P., Valls Miro, J., Perez-Vidal, C., and Tornero, J., 2019. "Robust hybrid position-force control for robotic surface polishing". *Journal of Manufacturing Science and Engineering,* ***141***(1).

[16] Dong, Y., Ren, T., Hu, K., Wu, D., and Chen, K., 2020. "Contact force detection and control for robotic polishing based on joint torque sensors". *The International Journal of Advanced Manufacturing Technology*, pp. 1–12.

[17] Ahn, J., Lee, M., Jeong, H., Kim, S., and Cho, K., 2002. "Intelligently automated polishing for high quality surface formation of sculptured die". *Journal of Materials Processing Technology,* ***130***, pp. 339–344.

[18] Ahn, J.-H., Shen, Y., Kim, H., Jeong, H.-D., and Cho, K.-K., 2001. "Development of a sensor information integrated expert system for optimizing die polishing". *Robotics and Computer-Integrated Manufacturing,* ***17***(4), pp. 269–276.

[19] De Agustina, B., Marín, M. M., Teti, R., and Rubio, E. M., 2018. "Analysis of force signals for the estimation of surface roughness during robot-assisted polishing". *Materials,* ***11***(8), p. 1438.

[20] Roswell, A., Xi, F. J., and Liu, G., 2006. "Modelling and analysis of contact stress for automated polishing". *International Journal of Machine Tools and Manufacture,* ***46***(3-4), pp. 424–435.

[21] Thomessen, T., Lien, T. K., and Sannæs, P. K., 2001. "Robot control system for grinding of large hydro power turbines". *Industrial Robot: An International Journal*.

[22] Kalt, E., Monfared, R., and Jackson, M., 2016. "Towards an automated polishing system: capturing manual polishing operations".

[23] Chen, S., Zhang, T., and Shao, M., 2017. "Interpolation optimization for robotic grinding with velocity constraints". *Advances in Mechanical Engineering,* ***9***(12), p. 1687814017708709.

[24] Dong, Y., Ren, T., Hu, K., Wu, D., and Chen, K., 2020. "Contact force detection and control for robotic polishing based on joint torque sensors". *The International Journal of Advanced Manufacturing Technology,* ***107***(5), Mar, pp. 2745–2756.

[25] Figliola, R. S., and Beasley, D. E., 2001. Theory and design for mechanical measurements.

[26] Harris, C. R., Millman, K. J., van der Walt, S. J., Gommers, R., Virtanen, P., Cournapeau, D., Wieser, E., Taylor, J., Berg, S., Smith, N. J., Kern, R., Picus, M., Hoyer, S., van Kerkwijk, M. H., Brett, M., Haldane, A., del Río, J. F., Wiebe, M., Peterson, P., Gérard-Marchant, P., Sheppard, K., Reddy, T., Weckesser, W., Abbasi, H., Gohlke, C., and Oliphant, T. E., 2020. "Array programming with NumPy". *Nature,* ***585***(7825), Sept., pp. 357–362.